This is a peer-reviewed, author's accepted manuscript of the following conference proceedings output:
Idarraga, G., Yang, L., Abad, F., Huang, Y., Dai, D., Xiao, Q., Lotfian, S., & Brennan, F. (Accepted/In press).
Hyperelastic modelling of elastomers for wave energy convertors.
In Proceedings of the ASME 2023 42st International Conference on Ocean, Offshore and Arctic Engineering [100523] ASME.

HYPERELASTIC MODELLING OF ELASTOMERS FOR WAVE ENERGY CONVERTORS

Guillermo Idarraga[1]*, Liu Yang[1], Farhad Abad[2], Yang Huang[2], Saishuai Dai[2], Qing Xiao[2], Saeid Lotfian[2], Feargal Brennan[2]

[1]Advanced Composite Group, Department of Mechanical and Aerospace Engineering, University of Strathclyde, 75 Montrose Street, Glasgow G1 1XJ, UK
[2]Department of Naval Architecture, Ocean and Marine Engineering, University of Strathclyde, Glasgow, UK
*Corresponding author: g.idarraga@strath.ac.uk

ABSTRACT

Flexible Wave Energy Converters (WECs) have gained considerable attention in recent years due to their ability to adapt to the dynamic conditions of the waves. To reach commercialization, further analyses should be done to guarantee survivability, and numerical models have been used to predict the structural response of WECs. However, the accuracy of any prediction will depend on the validity of the hyperelastic model employed and the reliability of the test data input into the chosen model. In this work, two elastomers are selected and characterised by plane stress, plane strain and biaxial stress conditions. Hyperelastic models are evaluated using ABAQUS, and hyperelastic constants are obtained for each elastomer. For the validation of the hyperelastic constants, experiments are conducted for one of the elastomers on the top of an oscillating water column (OWC) WEC. From the experiments, the deformation of the elastomeric membrane under wave conditions is obtained and compared with the results of a numerical model using the hyperelastic constants. From the results, the hyperelastic models describe well the deformation trend of the membrane on the top of the OWC, however further analysis should be done to improve the accuracy of the models.

Keywords: Flexible WECs, Hyperelastic models, Elastomers, Material characterisation.

1. INTRODUCTION

In comparison with other renewable energy technologies like solar or wind, the cost of wave energy is much higher, making difficult the commercialisation of WEC devices [1]. To increase the reliability and cost-effectiveness of WECs, different problems, such as survivability of the devices, fatigue life, maintenance, complex shapes, and device mass, should be solved [2]. Marine environments are challenging and dynamic contexts for devices. The structures should support high-energy storms with continual wetting and drying environment with salt-saturated water and intense solar radiation. For this reason, manufacturers have traditionally opted for rigid materials like metals and concrete. However, those heavy devices have demonstrated severe logistical problems and high manufacturing costs [3,4]. Metallic types of machinery have poor adaptability to wave conditions, resulting in high loads and premature fatigue failures, as well as corrosive mechanisms [5,6]. In most cases, designs are large and over-engineered to meet reliability standards, reducing cost-effectiveness.

Considering the current challenges of wave energy generation, in recent years, there has been a strong trend in the development of flexible WECs. New designs focus on flexible bodies have shown better adaptability to the dynamic conditions of the sea. Most designs are a single body structure with further reduced parts and joints compared with conventional WECs [7-10]. The characteristics of flexible WECs contribute to higher fatigue life, reliability, and survivability, addressing lower logistic costs due to their reduced weight structures [11-13]. Additionally, new researchers have demonstrated the possibility to integrate the Power-Take Off (PTO) generator into the flexible body using Dielectric Elastomers Generators (DEGs) [4,11,14,15].

Elastomers have different benefits, including high elongation, damping coefficient and fatigue life, which contribute to survivability. However, elastomers suffer from reduced tensile strength and low stiffness. Even though elastomers are widely used in marine structures such as fenders, buoys, boats and mooring lines, material selection and mechanical characterisation of elastomers have not been widely explored for WECs. A better characterisation of elastomers will allow for improving the accuracy of numerical models where material properties are required to analyse structural integrity, deformation, and power generation of WECs [16-17]. The accuracy of numerical predictions depends on the validity of the so-called hyperelastic model employed and the reliability of the test data input into the chosen model.

In this work, two elastomers are selected, and mechanical properties are characterised. Test data is acquired under conditions of plane stress (uniaxial tests), plane strain (planar tests) and equi-biaxial stress (biaxial tests). Based on the mechanical results, hyperelastic models are evaluated using ABAQUS and validated through experiments using an oscillating water column (OWC) WEC.

2. MATERIALS

Considering the huge universe of polymers and the wide range of properties and applications, two elastomers are identified for this work: natural rubber and styrene-butadiene. Natural rubber and styrene-butadiene are used in applications where durability under complex loading scenarios, a high number of fatigue cycles and high resilience are required.

Table 1 indicates some characteristics of the rubbers selected according to the providers. Latex (LTR) is a natural rubber provided by the company PAR Group UK. Latex has been widely used in WECs prototypes with DEGs under the commercial name of Theraband or OPPO band [18-20]. On the other hand, styrene-butadiene rubber (SBR) is a synthetic elastomer provided by the company Coruba UK. This rubber is used in different applications, including car and truck tires, belts, hoses, and footwear, among others.

TABLE 1: RUBBERS SELECTED AND SOME PROPERTIES PROVIDED IN THE DATASHEET.

Type	Thickness [mm]	Hardness	Strength [MPa]	Failure Strain [%]
LTR	0.38	35 Shore Micro	25.0	850
SBR	3.00	60 Shore A	11.3	450

3. MECHANICAL CHARACTERISATION

This section evaluates the elastomers under uniaxial, biaxial and planar conditions, which correspond to the main mechanical tests to characterise hyperelastic materials. The information in terms of stress and strain response will be obtained to determine the hyperelastic constants in the following section. The information corresponds to the engineering stress and strain, considering the initial area and length of the samples. Engineering stresses are more conservative when the strength of a material is measured, additionally, material coefficients of the hyperelastic models are calculated in ABAQUS based on engineering-stress-strain data [21]. All the tests are conducted using a computer-controlled Testomestric 500X-50 type universal servo-electric test machine with a regularly calibrated 50 kN rated load cell.

3.1 Uniaxial tests

The tests are carried out on dumbbell-shaped specimens prepared according to ASTM D412/ISO 37 [22]. At least five samples of each elastomer are evaluated. For the tests, self-tightening grips are used, and the displacement is measured through a long travel extensometer, see Figure 1. The tests are conducted at ambient temperature at a constant crosshead speed of 100 mm/min.

FIGURE 1: SETUP FOR UNIAXIAL TESTS FOR LTR.

Figure 2 shows the experimental results for uniaxial tests. It is observed that SBR has much higher stiffness and strength than LTR. This is because SBR has a much more complex chemical structure than LTR. The benzene group in the styrene makes it more difficult for the chains to rotate, uncoil, disentangle, and deform by viscous flow when stress is applied. On the other hand, in linear chemical structures like LTR, the chains rotate and slide easier when stress is applied, leading to reduced stiffness and strength. For this work and the calculation of hyperelastic constants, the response of the elastomers is analysed until 1.5 of strain, however, both elastomers can reach much higher strains. This strain is selected to capture a good amount of deformation of the material based on the OWC experiments in section 5.

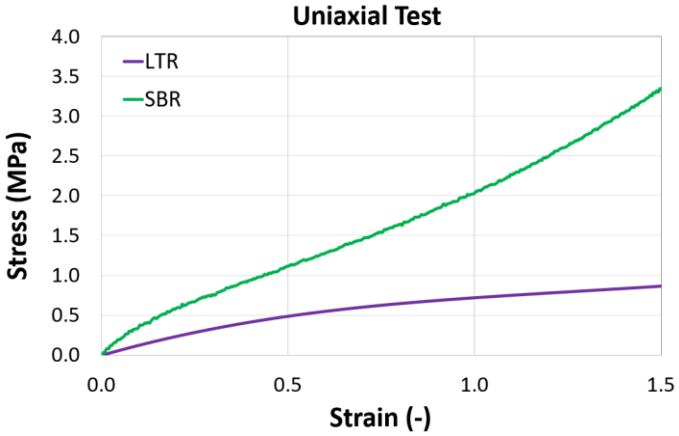

FIGURE 2: STRESS-STRAIN CURVES OF THE ELASTOMERS EVALUATED IN THE UNIAXIAL TEST.

3.2 Planar tests

The planar tension test imposes plane strain conditions on the test specimen by preventing lateral strains. Experiments are carried out using samples with a high aspect ratio. Therefore, the width of the specimens is considerably larger than the grip separation. For these tests, rectangular-shaped specimens are

used with a width of 200mm and a grip separation of 50mm, and five samples of each elastomer are evaluated. The tests are conducted at a constant crosshead speed of 50 mm/min. Due to the dimension of the samples, the deformation is measured using a Qualysis Oqus 300+ optical measurement system based on the reflection of infrared light of 6 dost taped in the samples, see Figure 3. The dots are separated horizontally by 60mm and vertically by 30mm, respecting each other. The displacement of the dots is tracked in longitudinal and lateral directions to guarantee the plane strain condition. Based on the results, lateral deformation of the samples is negligible, whereby, the plane strain condition is confirmed. The results of planar tests are shown in Figure 4, showing a non-linear plane strain response where SBR has the higher stiffness and loading carrying capacity. For the calculation of hyperelastic constants, the maximum strain used is 0.6, as Figure 4 shows. This strain is chosen based on the maximum strain of SBR obtained in the biaxial test.

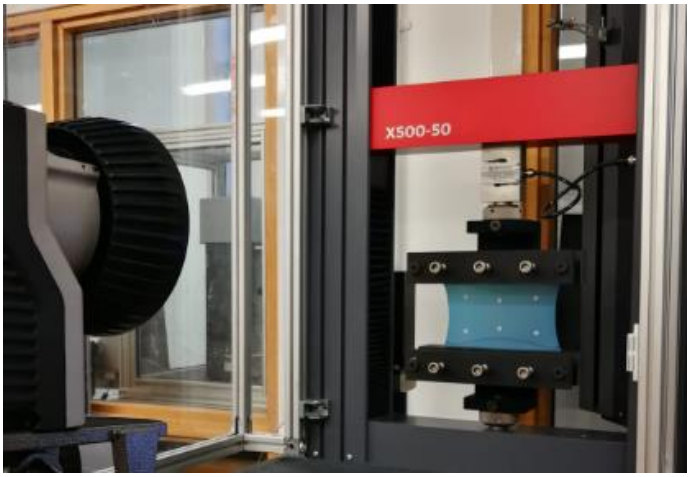

FIGURE 3: SETUP FOR PLANAR TESTS FOR LTR USING QUALYSIS OPTICAL MEASUREMENT SYSTEM.

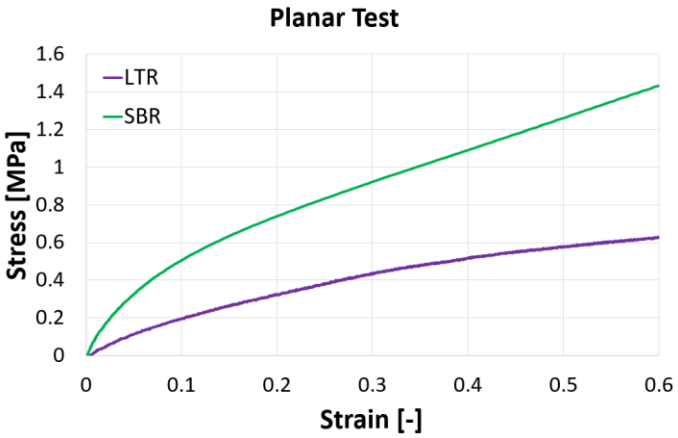

FIGURE 4: STRESS-STRAIN CURVES OF THE ELASTOMERS EVALUATED IN THE PLANAR TEST.

3.3 Biaxial tests

The equi-biaxial stress state is obtainable by stretching a square sheet in a biaxial test machine. For these tests, a biaxial scissor arm fixture to fit in the tensile test machine is used, see Figure 5. Duncan et al. demonstrated in [23] that this fixture is able to produce the same stresses in both of the principal axes, making this fixture reliable for biaxial tests. The specimens used in the biaxial tests are prepared from 45mm squares. A constant crosshead speed of 50 mm/min is used for the tests. Similar to planar tests, the deformation is measured using a Qualysis Oqus 300+ optical measurement system based on the reflection of infrared light of 4 dots taped in the samples, as Figure 5 shows. The results of biaxial tests are shown in Figure 6, indicating non-linear behaviour for both elastomers with a maximum strain of 0.6, which corresponds to the maximum strain of SBR before the sample starts to slide within the grips.

FIGURE 5: SETUP FOR BIAXIAL TESTS FOR LTR USING QUALYSIS OPTICAL MEASUREMENT SYSTEM.

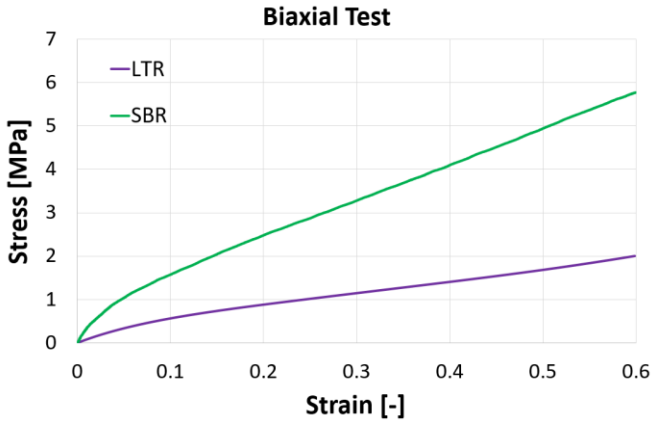

FIGURE 6: STRESS-STRAIN CURVES OF THE ELASTOMERS EVALUATED IN BIAXIAL TEST.

4. HYPERELASTIC MODELLING

In this section, the data obtained from the mechanical characterisation under the different loading conditions is implemented to obtain the hyperelastic models using ABAQUS hyperelastic material curve fitting capability. For the analysis, it is considered that the materials are fully incompressible rubbers.

For this analysis, Mooney-Rivlin and Ogden [24,25,26] with strain energy potential order one are used to describe the behaviour of the elastomers. Equations (1) and (2) introduce the strain-energy function W for Mooney-Rivlin and Ogden models respectively. Where C_{10}, C_{01}, μ_I and α_I are material constants that control shear behaviour, D_1 is the material constant that controls bulk compressibility, I_1 and I_2 are invariants which depend on the principal stretches λ_1,λ_2,λ_3 and the loading mode, and finally, J_{el} is elastic volume ratio. For this analysis, the third and second terms of Equations (1) and (2) are negligible since the material is considered fully incompressible.

$$W = C_{10}(I_1 - 3) + C_{01}(I_2 - 3) + \frac{1}{D_1}(J_{el} - 1)^2 \qquad (1)$$

$$W = \frac{2\mu_1}{\alpha_1^2}\left(\lambda_1^{\alpha_1} + \lambda_2^{\alpha_1} + \lambda_3^{\alpha_1} - 3\right) + \frac{1}{D_1}(J_{el} - 1)^2 \qquad (2)$$

Based on the strain-energy function W the principal stretches λ_i (i from 1 to 3) are related to the principal stresses using the Cauchy Stresses function, equation (3):

$$\sigma_i = \lambda_i \frac{\partial W}{\partial \lambda_i} \qquad (3)$$

ABAQUS generates an equation for each stress-strain data pair provided from the experiments and proposes a single set of hyperelastic constants to fit the experimental data. The set of hyperelastic constants generated by ABAQUS corresponds to the group of constants which best fit all the loading modes used in the analysis, i.e., uniaxial, planar and biaxial curves of section 3. Table 2 and Table 3 summarise the hyperelastic constants for LTR and SBR, respectively. All the models show stable behaviour, except for Mooney-Rivlin in the case of SBR, where it is possible to observe a reduction in the stress in Figure 7 as strain increases, leading to an unstable response for this model.

In the case of SBR, both models have poor fitting with experimental results (Figure 7 to Figure 9), especially for uniaxial behaviour. This is because Mooney-Rivlin and Ogden, with strain energy potential order one, do not capture well the upturn of the stress-strain relation in the uniaxial test for SBR after 0.3 of strain. Additionally, due to ABAQUS provides a single set of hyperelastic constants for all the loading conditions; the fitting capability is reduced, considering that the nature of the experiments differs between each other.

On the other hand, for LTR, the hyperelastic models provide a better correlation to the experimental curves, Figure 7 to Figure 9. LTR does not present an upturn of the stress-strain relation in the strain range considered in this work. However, it is common to observe an upturn (stiffening) in natural rubbers at much higher strains due to strain crystallisation. Both models show similar stress-strain responses in all the loading conditions, being equivalent to each other, observing a better fitting at lower strains.

TABLE 2: SET OF HYPERELASTIC CONSTANTS TO REPRODUCE UNIAXIAL, PLANAR AND BIAXIAL BEHAVIOUR FOR LTR.

Mooney-Rivlin			STABLE
D_1	C_{10} [MPa]	C_{01} [MPa]	
0	-8.43E-03	2.95E-01	

Ogden			STABLE
D_1	μ_I [MPa]	α_I	
0	5.87E-01	-1.88E+00	

TABLE 3: SET OF HYPERELASTIC CONSTANTS TO REPRODUCE UNIAXIAL, PLANAR, AND BIAXIAL BEHAVIOUR FOR SBR.

Mooney-Rivlin			UNSTABLE
D_1	C_{10} [MPa]	C_{01} [MPa]	
0	-1.97E-01	8.84E-01	

Ogden			STABLE
D_1	μ_I [MPa]	α_I	
0	1.35E+00	-2.33E+00	

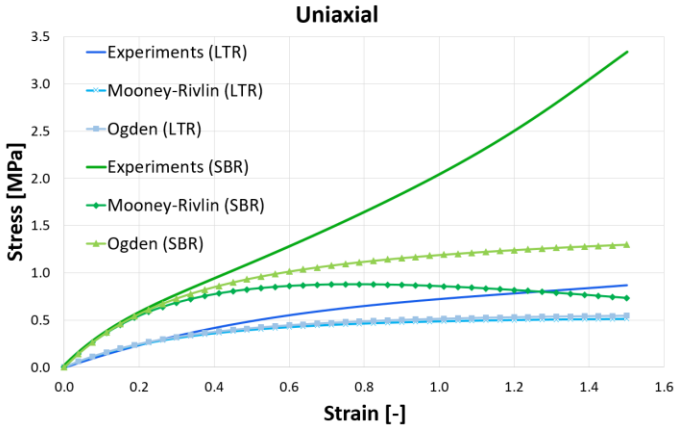

FIGURE 7: FITTING OF THE HYPERELASTIC MODELS WITH UNIAXIAL EXPERIMENTAL DATA.

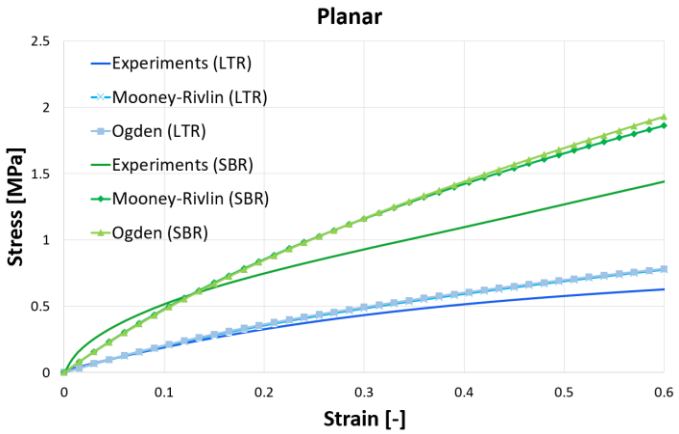

FIGURE 8: FITTING OF THE HYPERELASTIC MODELS WITH PLANAR EXPERIMENTAL DATA.

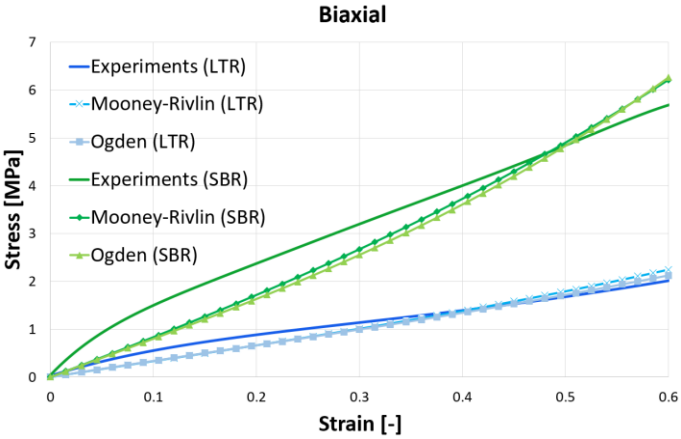

FIGURE 9: FITTING OF THE HYPERELASTIC MODELS WITH BIAXIAL EXPERIMENTAL DATA.

5. OWC EXPERIMENTS AND VALIDATION

As mentioned previously, for the validation of the hyperelastic models, a water tank experiment is conducted for LTR on the top of an OWC WEC. This experiment is conducted in the 3D compact wave tank (9.575m × 3.150m × 1.000m) of the Kelvin Hydrodynamic Laboratory (KHL) of the University of Strathclyde. The OWC model and its dimensions are shown in Figure 10.

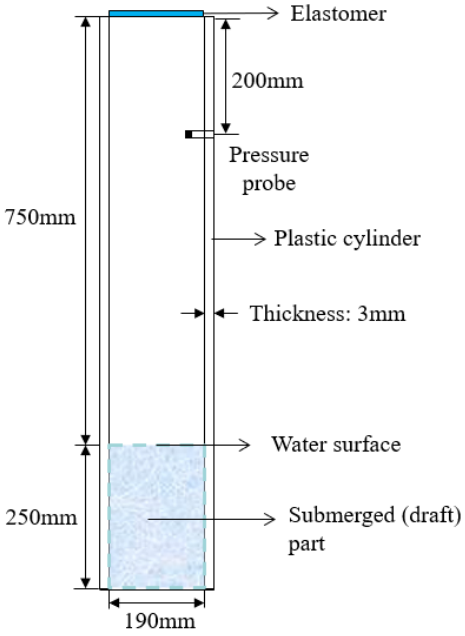

a)

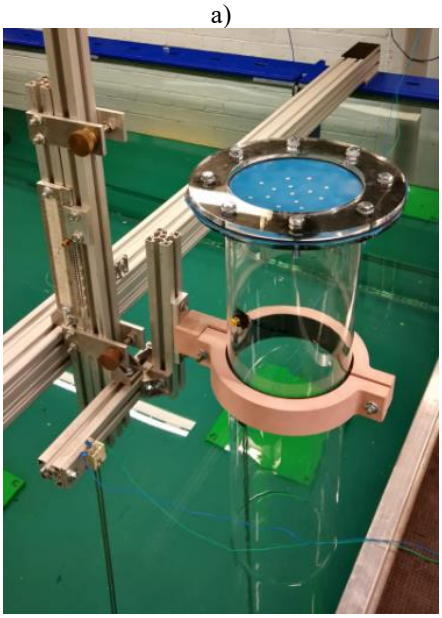

b)

FIGURE 10: A) DIMENSIONS OF OWC AND MEMBRANE PART, B) SPECIMEN WITH MARKERS

Qualysis Oqus 300+ optical measurement system with two cameras is set above the cylinder. The deformation is measured using infrared light and specific markers stuck to the membrane. A pressure transducer (Honeywell 163PC01D75) is attached near the top of the cylinder to measure the pressure inside the air chamber. In the water tank, regular waves with an amplitude of 0.01m and a frequency of 0.375 Hz are generated.

In this study, instead of using the coupled fluid-structure interaction analysis method based on computational fluid dynamics (CFD), a finite element-based analysis is carried out in

ABAQUS to calculate the deformation of the elastomer in the centre of the membrane (tip displacement) and validate the hyperelastic models. For validation, the hyperelastic constants obtained from LTR in the previous section are implemented in the material description in ABAQUS. In this simulation, pressure transducer data is applied as the loading condition, and the elastomer is modelled using 4-node bilinear axisymmetric quadrilateral elements (CAX4H). Figure 11 shows the model implemented in Abaqus, which corresponds to an axisymmetric 2D model.

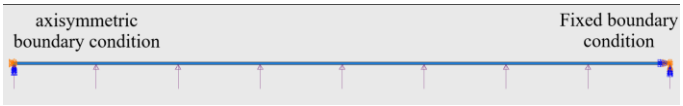

FIGURE 11: NUMERICAL MODEL OF THE OWC IN ABAQUS.

The numerical results using the hyperelastic constants and the experimental results obtained from the wave tank test are shown in Figure 12. It is possible to observe that the numerical analysis using Mooney-Rivlin and Ogden hyperelastic models reproduces the deformation trend of the membrane. However, there is a difference in the maximum displacement of the membrane between the numerical and the experimental results, where the numerical model overestimates the tip displacement. These results agree with the differences found between hyperelastic models and experimental results in section 4 (Figure 7 to Figure 9), where the models show higher strains at specific stresses.

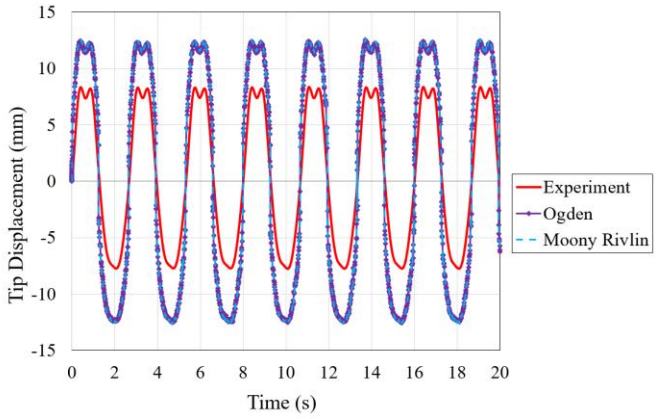

FIGURE 12: COMPARISON BETWEEN NUMERICAL MODEL USING HYPERELASTIC CONSTANTS AND EXPERIMENTAL RESULTS OBTAINED FROM THE OWC IN THE WATER TANK.

6. CONCLUSION

Hyperelastic models are useful tools to describe the behaviour of elastomers under different loading conditions allowing the modelling of flexible structures of WECs. However, the reliability of the hyperelastic constants depends directly on the mechanical characterisation and the data input in the analysis. In this case, a poor fitting of the hyperelastic models is obtained for SBR using Mooney-Rivlin and Ogden with strain energy potential order 1, which suggests that a higher-order model should be used to describe the upturn of the stress-strain relation of the material in the uniaxial condition. On the other hand, as a single set of hyperelastic constants is provided by ABAQUS to describe the combination of loading conditions, the fitting capability is reduced. An analysis where hyperelastic constants are generated separately for each loading mode could improve the fitting of the hyperelastic model with the experimental curve, but the model would limit to the loading condition used.

From the validation of the hyperelastic constants of LTR, the numerical model described well the deformation trend of the membrane on the top of the OWC. The model accuracy needs to be improved since it overestimated the displacement of the tip. This could be achieved by obtaining a set of hyperelastic constants for an independent loading mode which describes the dominant loading condition in the OWC and/or improving the analysis of the material, including volumetric tests to describe the bulk compressibility of the elastomer, as it is suggested in [21].

ACKNOWLEDGEMENTS

This research is supported by an EPSRC Grant “Bionic Adaptive Stretchable Materials for WEC (BASM-WEC)” (No. EP/V040553/1).

REFERENCES

[1] Seanergy, 2016. Ocean Energies, Moving towards Competitiveness: a Market Overview.

[2] Materials Landscaping Study – Final Report. WES_LS01_ER_Materials.

[3] Koca K, Kortenhaus A, Oumeraci H, et al. Recent Advances in the Development of Wave Energy Converters. The 10th European Wave and Tidal Enhergy Conference (EWTEC 2013), Aalborg, Denmark.

[4] Collins I, Hossain M, Dettmer W, Masters I. Flexible membrane structures for wave energy harvesting: A review of the developments, materials and computational modelling approaches. Renewable and Sustainable Energy Reviews 151 (2021) 111478.

[5] Yemm R, Pizer D, Retzler C, Henderson R. Pelamis: experience from concept to connection. Phil Trans R Soc A 2012;370(1959):365–80.

[6] Lin Y, Bao J, Liu H, Li W, Tu L, Zhang D. Review of hydraulic transmission technologies for wave power generation. Renew. Sustain. Energy Rev. 50, 194–203, 2015b.

[7] Orphin J, Fleming A, Algie C. Physical scale model testing of a flexible membrane wave energy converter: Videogrammetric analysis of membrane operation. International Journal of Marine Energy 20 (2017) 135–150.

[8] Alam M.R. A flexible seafloor carpet for high-performance wave energy extraction. Proceedings of OMAE 2012. 31st International Conference on Ocean, Offshore and Arctic Engineering. June 10-15, 2012, Rio de Janeiro, Brazil.

[9] Kurniawan A, Chaplin J.R, Greaves D.M, Hann M. Wave energy absorption by a floating air bag. Journal of Fluid Mechanics , Volume 812 , 10 February 2017 , pp. 294 – 320.

[10] Babarit A, Wendt F, Yu Y.H, Weber J. Investigation on the energy absorption performance of a fixed-bottom pressure-differential wave energy converter. Applied Ocean Research 65 (2017) 90–101.

[11] Jean P, Wattez A, Ardoise G, et al. Standing Wave Tube Electro Active Polymer Wave Energy Converter. Proc. of SPIE Vol. 8340 83400C-1, 2012.

[12] Technology Description and Status Electric Eel. Knowledge Capture Project, AWS Project No 15-007.

[13] Chaplin J.R, Heller V, Farley F.J.M, Hearn G.E, Rainey R.C.T. Laboratory testing the Anaconda. Phil. Trans. R. Soc. A (2012) 370, 403–424.

[14] Moretti G, Herran M.S, Forehand D, et al. Advances in the development of dielectric elastomer generators for wave energy conversion. Renewable and Sustainable Energy Reviews 117 (2020) 109430.

[15] Maas J, Graf C. Dielectric elastomers for hydro power harvesting. Smart Mater. Struct. 21 (2012) 064006 (12pp).

[16] McDonald A, Xiao Q, Forehand D, Costello R. Linear analysis of fluid-filled membrane structures using generalised modes. Proceedings of the 13th European Wave and Tidal Energy Conference 1-6th Sept 2019, Naples, Italy.

[17] Li X, Xiao Q, Luo Y, Moretti G, Fontana M, Righi M. Dynamic response of a novel flexible wave energy converter under regular waves. Proceedings of the 14th European Wave and Tidal Energy Conference 5-9th Sept 2021, Plymouth, UK.

[18] Righi M, Moretti G, Forehand D, et al. A broadbanded pressure differential wave energy converter based on dielectric elastomer generators. Nonlinear Dyn 105, 2861–2876 (2021). https://doi.org/10.1007/s11071-021-06721-8

[19] PolyWEC project. Final publishable summary report. Grant Agreement number: 309139.

[20] Kaltseis R, Keplinger C, Koh S.J.A, et al. Natural rubber for sustainable high-power electrical energy generation. RSC Adv 2014;4(53). pp. 27 905–927 913.

[21] Dassault Systemes ABAQUS 2016, Analysis user's guide volume iii: materials. Hyperelastic behavior of rubberlike materials. Section 22.5.1–10.

[22] ASTM D412-16(2021), Standard Test Methods for Vulcanized Rubber and Thermoplastic Elastomers—Tension

[23] Duncan B.C, Maxwell A.S, Crocker L.E, Hunt R. Verification of hyperelastic test methods. Teddington: NPL; 1999. NPL Report CMMT(A) 226.

[24] Mooney M, A. theory of large elastic deformation, Journal of Applied Physics 11 (9) (1940) 582–592.

[25] Rivlin R.S. Large elastic deformations of isotropic materials IV. Further developments of the general theory, Philosophical Transactions of the Royal Society of London – Series A 241 (835) (1948) 379–397

[26] Ogden R.W. Large deformation isotropic elasticity. On the correlation of theory and experiment for incompressible rubber-like solids, Philosophical Transactions of the Royal Society of London – Series A 326 (1972) 565–584.